



**HAL**  
open science

# Experimental calcite dissolution under stress: Evolution of grain contact microstructure during pressure solution creep

Delphine Croizé, François Renard, Knut Bjørlykke, Dag Kristian Dysthe

## ► To cite this version:

Delphine Croizé, François Renard, Knut Bjørlykke, Dag Kristian Dysthe. Experimental calcite dissolution under stress: Evolution of grain contact microstructure during pressure solution creep. *Journal of Geophysical Research*, 2010, 115, pp.09207. 10.1029/2010JB000869 . insu-00549096

**HAL Id: insu-00549096**

**<https://insu.hal.science/insu-00549096>**

Submitted on 10 Mar 2021

**HAL** is a multi-disciplinary open access archive for the deposit and dissemination of scientific research documents, whether they are published or not. The documents may come from teaching and research institutions in France or abroad, or from public or private research centers.

L'archive ouverte pluridisciplinaire **HAL**, est destinée au dépôt et à la diffusion de documents scientifiques de niveau recherche, publiés ou non, émanant des établissements d'enseignement et de recherche français ou étrangers, des laboratoires publics ou privés.

## Experimental calcite dissolution under stress: Evolution of grain contact microstructure during pressure solution creep

Delphine Croizé,<sup>1,2</sup> François Renard,<sup>2,3</sup> Knut Bjørlykke,<sup>1</sup> and Dag Kristian Dysthe<sup>3</sup>

Received 14 January 2010; revised 6 May 2010; accepted 18 May 2010; published 15 September 2010.

[1] For the first time, nanometer resolution techniques both in situ and ex situ were compared in order to study calcite dissolution under stress. The obtained results enabled identification of the relative importance of pressure solution driven by normal load and free surface dissolution driven by strain energy. It is found that pressure solution of calcite crystals at the grain scale occurred by two different mechanisms. Diffusion of the dissolved solid took place either at a rough calcite/indenter interface, or through cracks that propagated from the contact toward the less stressed part of the crystal. It is also found that strain rates are mostly a function of the active process, i.e., pressure solution associated or not with cracks, rather than being influenced by stress variations. Strain rates obtained in this study are in agreement with published data of experimental calcite and carbonate dissolution under stress.

**Citation:** Croizé, D., F. Renard, K. Bjørlykke, and D. K. Dysthe (2010), Experimental calcite dissolution under stress: Evolution of grain contact microstructure during pressure solution creep, *J. Geophys. Res.*, 115, B09207, doi:10.1029/2010JB000869.

### 1. Introduction

[2] During burial, sediments are subjected to increasing stresses and temperature with depth. Their compaction results in a porosity decrease and an increase in density. Compaction processes may be either mechanical and thus a function of the effective stress, or chemical, involving dissolution and precipitation of minerals. Pressure solution creep is a chemical deformation mechanism occurring in the presence of a reactive fluid, and is responsible for slow and irreversible compaction of sediments. Intergranular pressure solution creep is an important process of porosity loss in sedimentary basins [Rutter, 1983; Tada and Siever, 1989] or of healing of active faults during the interseismic period [Ramsay, 1980; Angevine et al., 1982; Gratier, 1987; Renard et al., 2000]. An other possible irreversible deformation mechanism during compaction of sediments is subcritical crack growth [Atkinson, 1982; Liteanu and Spiers, 2009].

[3] Pressure solution is driven at the microscale by chemical potential differences between the stressed and unstressed part of the solid which cause (1) dissolution of minerals along the contact, (2) diffusion toward the pore space, and (3) precipitation on the less stressed faces of the grains [Sorby, 1863; Weyl, 1959]. The overall rate of deformation is controlled by

the slowest of these three processes. Pressure solution may therefore be controlled by the kinetics of either dissolution or precipitation reactions, or by the rate of diffusion along the grain boundary. Diffusive transport along the grain contact is driven by the chemical potential gradient existing between the liquid in the contact and the one in the pore space, the rate of transport also depends on the geometry, i.e., thickness and microstructure, of the grain-to-grain contact.

[4] Theoretical relations describing the strain rate of aggregates compacting by intergranular pressure solution include phenomenological coefficients [Weyl, 1959; Lehner, 1990]. They also have different dependencies on grain size and stress according to whether the process is controlled by kinetics or by diffusion. A number of experimental studies have been carried out to determine these parameters, but few experimental data exist on calcite pressure solution creep. Recent experimental studies were carried on both fine-grained (3 to 80  $\mu\text{m}$ ) super-pure calcite powder compacted at 2–4 MPa effective stress [Zhang et al., 2002; Zhang and Spiers, 2005a, 2005b] and at 30 MPa [Liteanu and Spiers, 2009] using an oedometer, and on calcite crystals indented by glass [Zubtsov et al., 2005]. Either the deformation was proposed to be controlled by diffusion [Zhang and Spiers, 2005a; Zubtsov et al., 2005] or by precipitation kinetics [Baker et al., 1980; Zhang et al., 2002; Zhang and Spiers, 2005b]. The lack of consensus on the rate-limiting process of pressure solution in carbonates is related to the absence of good agreement between macroscopic strain rate laws and experimental results. A possible explanation is that present models do not take grain size distribution or packing of aggregates accurately into account. In addition, the grain-to-grain geometry employed in the macroscopic models might not be suitable for carbonates.

<sup>1</sup>Department of Geosciences, University of Oslo, Blindern, Oslo, Norway.

<sup>2</sup>Laboratoire de Géodynamique des Chaînes Alpines, Université Joseph Fourier-Grenoble I, CNRS-Observatoire de Grenoble, Grenoble, France.

<sup>3</sup>Physics of Geological Processes, University of Oslo, Blindern, Oslo, Norway.

**Table 1.** Experimental Conditions and Results From in Situ and White Light Interferometry Measurements<sup>a</sup>

No	Conditions						In Situ Measurements						WLI Measurements						
	$e$ ( $\mu\text{m}$ )	IM	$R$ (mm)	$R^*$ (mm)	$R_{res}$ (mm)	$F$ (N)	$S_1$ ( $\mu\text{m}^2$ )	$\sigma_1$ (MPa)	$Z_f$ ( $\mu\text{m}$ )	$V_f$ ( $\mu\text{m}^3$ )	$t_f$ (hours)	$S_f$ ( $\mu\text{m}^2$ )	$Z_p$ ( $\mu\text{m}$ )	$V_p$ ( $\mu\text{m}^3$ )	$Z_{fwi}$ ( $\mu\text{m}$ )	$V_{fwi}$ ( $\mu\text{m}^3$ )	$h$ ( $\mu\text{m}$ )	Duration (hours)	$S_{fwi}$ ( $\mu\text{m}^2$ )
F01	300	glass	0.77	1.60	1.27	1.15	2650	434	0.19	184	26.08	3603	0.085	28.90	0.84	5610.9	0.60	64.20	2169
F02	567	glass	0.50	1.04	1.27	1.14	1974	578	0.08	23.2	34.01	2090	0.083	27.70	0.52	2069.6	0.21	52.61	785
F03	580	glass	0.25	0.52	0.37	0.88	1065	826	0.02	0.79	24.44	1086	0.340	134.3	0.07	353.9	0	28.44	973
F05	510	glass	0.50	1.04	1.25	1.08	1397	773	0.06	12.8	28.50	2363	0.075	21.90	0.67	4592.1	0.45	40.51	1335
F06	153	glass	0.50	1.04	1.33	1.46	3327	439	0.12	46.4	37.42	3492	0.160	113.4	0.05	2592.6	2.58	90.42	1169
F07	682	sapphire	0.50	2.70	0.96	1.27	1572	808	0.05	20.4	46.75	1823	0.120	43.43	0.20	1225.2	0.60	49.88	777

<sup>a</sup>Parameters are  $e$ , thickness of the calcite crystal used; IM, indenter material;  $S_1$ ,  $S_f$  initial and final surface area of contact calculated from in situ pictures;  $\sigma_1$ , Initial stress  $\sigma_1 = F/S_1$ ;  $Z_f$ ,  $V_f$  the subscript  $f$  denotes values obtained from the last picture,  $Z_f$  has an accuracy of  $\pm 0.009 \mu\text{m}$ ;  $t_f$ , time of the last picture used to determine in situ vertical displacement;  $Z_{fwi}$  has an accuracy of  $\pm 0.003 \mu\text{m}$ ; and Duration, total duration of the experiments.

[5] Macroscopic predictive theories describing aggregate compaction by pressure solution creep should be based on spatial averaging methods using microscale phenomenological descriptions [Lehner, 1990]. Therefore, to predict the strain rate at aggregate or outcrop scale, a good understanding of the three serial processes at the grain scale and of the detailed microstructure of the grain contact is required. The structure of grain-to-grain contact and its effect on the rate of pressure solution creep are still not fully understood, however. Several types of grain boundary structures are debated in the literature [Tada and Siever, 1986; Gratz, 1991; De Meer and Spiers, 1999; Dysthe et al., 2002; van Noort et al., 2008]. Pressure solution might occur as a combination of plastic deformation at the grain-to-grain contact and free face dissolution at the edge of the contact [Tada and Siever, 1986; Karcz et al., 2006]. A number of studies have assumed that water is present at the grain boundary and have discussed several geometries. For instance the grain boundary may be flat and diffusion occurs through an adsorbed thin film which can support shear stresses [Weyl, 1959; Rutter, 1983; Yasuhara et al., 2003] and has a slightly smaller diffusion coefficient than a free fluid. Another type of grain contact geometry is the dynamic island and channel structure [Raj, 1982; Lehner, 1990], where stresses are transmitted through solid-solid contacts. In this model, the fluid is at hydrostatic pressure and has transport properties similar to the pore fluid. A third type of structure is a thin film, short-circuited by crack arrays [Gratz, 1991; den Brok et al., 2002].

[6] Another process, that is less understood, is the formation of tiny cracks that grow slowly and permanently damage the solid [Atkinson, 1982]. The propagation of such cracks at stress intensity factor lower than the critical stress intensity factor is called subcritical crack growth or stress corrosion. The three important variables to be taken into account are the applied stress, the size of the flaw and the fracture toughness [Anderson, 1995; Scholz, 2002]. Following the energy criterion theory, cracks will propagate in order to lower the total energy of the system [Griffith, 1921]. The driving force for crack propagation is the energy release rate which corresponds to the change in potential energy with crack surface area for a linear elastic material. At equilibrium the energy release rate is proportional to the material resistance to cracking, which is also equivalent to the surface energy, therefore the material resistance to cracking is affected by the environment [Olagnon et al., 2006]. Due to the preexistence of flaws in the rocks, crack propagation may occur at stresses lower than required for

slip or twinning [Atkinson, 1982; Olagnon et al., 2006], and the presence of water at the crack tip may promote weakening reactions.

[7] Grain contact healing, or neck growth, has been showed to be a mechanism taking place in pressure solution experiments where both the indenter and the indented material were halite [Hickman and Evans, 1991; Zubtsov et al., 2004; van Noort et al., 2007], this is possibly an important mechanism for calcite as well [Yamasaki and Weiping, 1993]. The present study aims at understanding the important connection between contact geometry and strain rate, however. To this end an experimental setup was designed, in which a point force is applied on a calcite crystal via a hemispherical lens made of either glass or sapphire, to study stress-enhanced dissolution along a single contact. A film of water saturated with respect to calcite is present at the calcite/lens interface. High stresses along the contact induce dissolution of calcite below the lens and, therefore, an increase of the contact surface area. The growth of the contact and the resulting displacement are followed during several tens of hours using optical interferometry, i.e., displacement of Newton rings. This allows the determination of the rate of calcite dissolution as a function of stress. Before and after experiments, crystal surface topography was measured down to nanometer resolution using white light interferometry, enabling determination of the resulting microstructures. The rates measured in the present study are compared with previous studies of calcite indentation or carbonate slow deformation.

## 2. Experimental Method

[8] A single indenter setup was specifically designed to study dissolution of calcite under stress, the method is similar to the one used by Hickman and Evans [1995]. First, Iceland spar calcite crystals were cleaved and polished to start each experiment with a flat crystallographic surface. The indented plane was normal to a cleavage and miscut with respect to the calcite rhombs. Calcite samples used were natural samples mined in southwest China and manufactured by Photox Optical System Ltd. Surface roughness was measured using white light interferometry prior to the force application. The surface area of the samples was close to  $2 \times 2 \text{ mm}^2$ . Sample thickness varied in the range 150–680  $\mu\text{m}$ . Second, a single contact force was applied on one point of the calcite crystal using a glass or sapphire half-ball lens provided by Edmund Optics. Half-balls with three different radii were used (Table 1), providing different initial

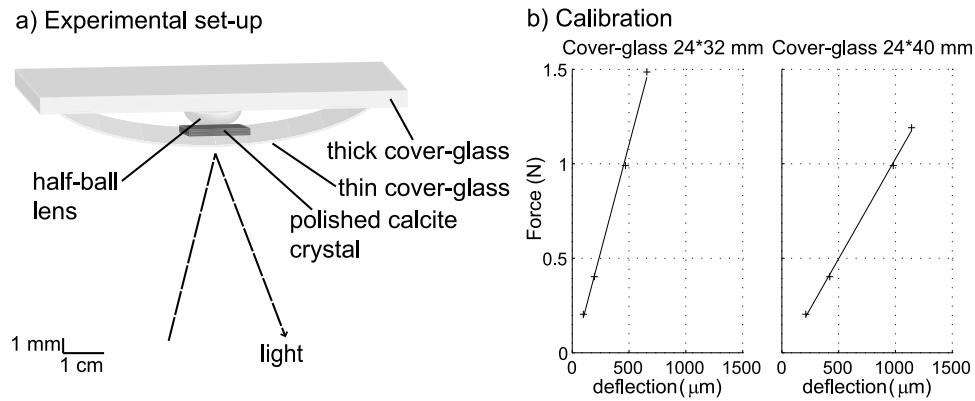


**Figure 1.** (a) Experimental setup. A flat piece of polished calcite crystal is pressed against a half-ball lens by means of a bent cover glass. (b) Force calibration. Deflection versus applied force relationships obtained for the two types of cover glasses used.

contact surface areas. The calcite crystal and the half-ball lens were placed between a thin cover glass bent over the half-ball lens and glued at both ends onto a thicker cover glass (as shown in Figure 1a). The applied force was a function of the bending of the thin cover glass, i.e., of the total height of half-ball lens and calcite crystal. Third, water saturated with respect to calcite was introduced in the system, i.e., after loading. After the water injection, the progression of the water at the calcite/lens interface and the complete wetting of the contact was observed with the microscope. Because the half-ball lenses were either made of glass or sapphire, these two materials being less reactive than calcite, they are assumed to be chemically inert. After validating the experimental protocol on a dozen test experiments, a series of six experiments was performed for which the experimental conditions are to be found in Table 1.

[9] The relationship between applied force and deflection of the thin cover glass was calibrated using two different cover glasses and four different dead weights (Figure 1b). Since the calcite samples in the experiments were glued onto the thin cover glass, calcite crystals of similar size were glued on the thin cover glasses during force calibration to ensure that the elastic parameters of the setup were similar. For calibration, a thin cover glass was initially maintained horizontally by two stands, one on each side. A dead weight was then suspended on the cover glass using a sewing needle. For each cover glass and weight, the deflection due to the suspended weight was measured using an LVDT LD400-5 displacement sensor provided by Omega Engineering Inc. The resulting deflection versus force curve was then used to determine the applied force,  $F$ , in each experiment (Figure 1b).

[10] The calcite/lens contact was observed using an inverted reflected light microscope (Olympus GX 71). The light source was a green monochromatic LED with a specific wavelength of  $\lambda = 530$  nm. Light was transmitted across the loaded sample, and interference fringes formed around the contact between the calcite sample and the half-ball lens. The light rays reflected from the lens/water and water/calcite interfaces produced concentric constructive (high intensity) and destructive (low intensity) interference fringes centered on the contact (Figure 2). These interference fringes are called Newton rings and were produced

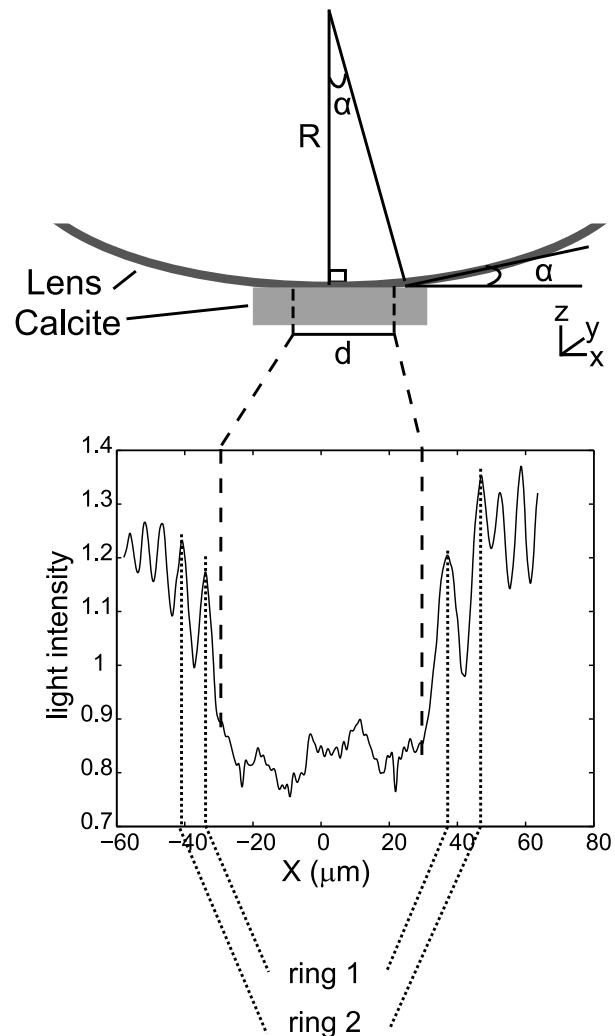


**Figure 2.** (top) Geometry of the calcite/half-ball lens interface. During experiments, a water film is present at the calcite/glass interface.  $R$ , radius of the half-ball lens used;  $d$ , contact diameter. (bottom) Light intensity (arbitrary units) along a 1D profile across the contact, showing constructive/destructive interference patterns.

when the distance between the two solids was of the same order of magnitude as the light wavelength [Tolansky, 1973]. The motion of the interference fringes due to the increase of the contact was followed for several tens of hours using time-lapse photography (D100 Nikon Digital Camera). The contact surface area,  $A$ , was extracted using image processing software (ImageJ), by outlining by hand the dark center of the picture enclosed within the first Newton ring. The applied stress was then simply calculated using  $\sigma = F/A$ . The picture resolution being  $\lambda/4$ , the actual surface area of contact might therefore be smaller than the one outlined by hand, which implies that the calculated stress values represent minimum values.

[11] At the beginning of each experiments, water saturated with respect to calcite was introduced at the calcite/lens interface with the help of a microsyringe. The high stress at the wetted calcite/lens interface induced a chemical potential gradient from the contact toward the nonstressed part of the fluid. The enlargement of the contact surface area resulted in a change of the setup geometry (Figure 2), and the displacement of the Newton rings could then be monitored. In some experiments the water film evaporated and a new saturated water droplet was injected in the contact and the time noted. This shows that the solutions are usually supersaturated during experiments.

[12] At the end of each experiment, the crystal was dried and the resulting surface topography was measured using white light interferometry (Wyko 2000 Surface Profiler from Veeco). This was done by means of a microscope with a reference arm creating interference fringes with maximum intensity at equal optical path lengths of the imaging beam and reference beam. By moving the sample vertically and simultaneously capturing an image of the interference intensity envelope, the relative height of the imaged surface at each pixel can be determined with a vertical resolution of 3 nm. The horizontal resolution depended on the lens used and was in the range 0.24 to 0.50  $\mu\text{m}$ . A detailed topography of the indented region was obtained from these measurements. The results are displayed as a digital elevation image in which the height range is shown as a color scale.

### 3. Data Analysis

#### 3.1. In Situ Measurements

[13] Color pictures of the contact and the Newton rings were taken at regular interval for a period of up to three days. Pictures were first split into the red, green and blue channels. Since a green light source was used, the green channel only was selected to get a better signal-to-noise ratio. In order to optimize the data visualization, contrast enhancement filters were also used. For each experiment, the lower and upper bounds of the recorded intensity were identified, then the same linear contrast stretch was applied on the whole set of pictures. To ensure that the Newton rings displacement was due to the contact dissolution and not to a movement of the entire crystal, a static reference point on the pictures was chosen and an image cross-correlation method was applied to the entire set of time-lapse pictures. If the cross correlation revealed an overall displacement of the setup, for instance due to microscope vibrations, the selected pictures were translated using the displacement vector obtained with the cross correlation.

[14] Figure 3 describes the successive data processing steps, which from the recorded pictures lead to the determination of the rate of contact surface area enlargement. A profile perpendicular to the Newton rings was chosen in each recorded picture, the profile was 10 pixels wide and stacked to suppress some noise. The selected intensity profile was smoothed using a Butterworth low-pass filter. Each profile was then centered such that the center of the contact area was located at  $X = 0$ . The evolution of the diameter with time was related to the increase of the contact surface area and hence to the decrease of the applied stress, i.e.,  $\sigma = F/A$  with  $F \approx \text{constant}$ .

[15] The volume of dissolved calcite is equal to the volume of the half-ball lens replacing solid calcite. To determine the volume of calcite dissolved through time, the vertical displacement of the half-ball lens was calculated at different time steps  $t_i$ . The vertical displacement occurring between  $t_{i-1}$  and  $t_i$  is expressed by  $\delta_{i,n}$ , with  $n$  the order of the interference fringe considered. Knowing the geometry of the setup (Figure 2) and the horizontal displacement of the  $n^{\text{th}}$  Newton ring, vertical displacement is calculated as follows:

$$\delta_{i,n} = (X_{i,n} - X_{i-1,n}) \tan \left[ \arcsin \left( \frac{X_{i-1,n}}{R^+} \right) \right], \quad (1)$$

where  $X_{i,n}$  is the distance from the considered Newton ring to the center of the contact area at  $t_i$  and  $R^+$  the equivalent radius of the half-ball lens calculated on the assumption that the contact between the half-ball lens of radius  $R$  and the calcite crystal follows the Hertz contact theory between two elastic bodies, with  $R^+ = (4Ea)/((1 - \nu^2)3\pi\sigma)$  [Fischer-Cripps, 1999].  $E$  and  $\nu$  are, respectively, the Young's modulus and Poisson's ratio of the half-ball lens,  $a = ((3FR)/(4E_r))^{1/3}$  is the calculated contact radius from Hertz contact theory, with  $E_r = ((1 - \nu_{\text{calcite}}^2)(E_{\text{calcite}}) + (1 - \nu_{\text{indenter}}^2)(E_{\text{indenter}}))^{-1}$ ,  $F$  being the applied force [Johnson, 1985]. To calculate  $E_r$ ,  $a$  and  $R^+$  the following elastic constants were used:  $\nu_{\text{calcite}} = 0.32$ ,  $E_{\text{calcite}} = 73$  GPa,  $\nu_{\text{glass}} = 0.25$ ,  $E_{\text{glass}} = 82$  GPa,  $\nu_{\text{sapphire}} = 0.25$  and  $E_{\text{sapphire}} = 335$  GPa.

[16] From  $\delta_{i,n}$  the total vertical displacement  $Z_{i,n}$  at  $t_i$  is then calculated as follows:

$$Z_{i,n} = \sum_{i=1}^j \delta_{i,n}. \quad (2)$$

[17] The largest source of error in the calculation of  $\delta_{i,n}$  according to this method lies in determining the minima of the fringes, i.e., the value of  $X_i$  on the picture. This error is typically  $\pm 3$  pixels, one pixel being equivalent to 0.118  $\mu\text{m}$ , it can be assumed that  $\delta_{i,n}$  is accurate at  $\pm 0.009$   $\mu\text{m}$ . This calculation implies the assumption that first the calcite surface is flat outside the contact and second, the calcite surface does not change outside the contact. The typical roughness over a crystal surface of 3000  $\mu\text{m}^2$  is about  $R_a = 50$  nm both before and after experiments. Therefore the accuracy of the vertical measurements  $Z$  can be assumed to be  $\pm 0.009$   $\mu\text{m}$ .

[18] The indenter used was a half-ball lens, therefore, the volume,  $V_{i,n}$ , of dissolved calcite is equal to the volume of a spherical cap,

$$V_{i,n} = \pi Z_{i,n}^2 \left( R^+ - \frac{Z_{i,n}}{3} \right). \quad (3)$$

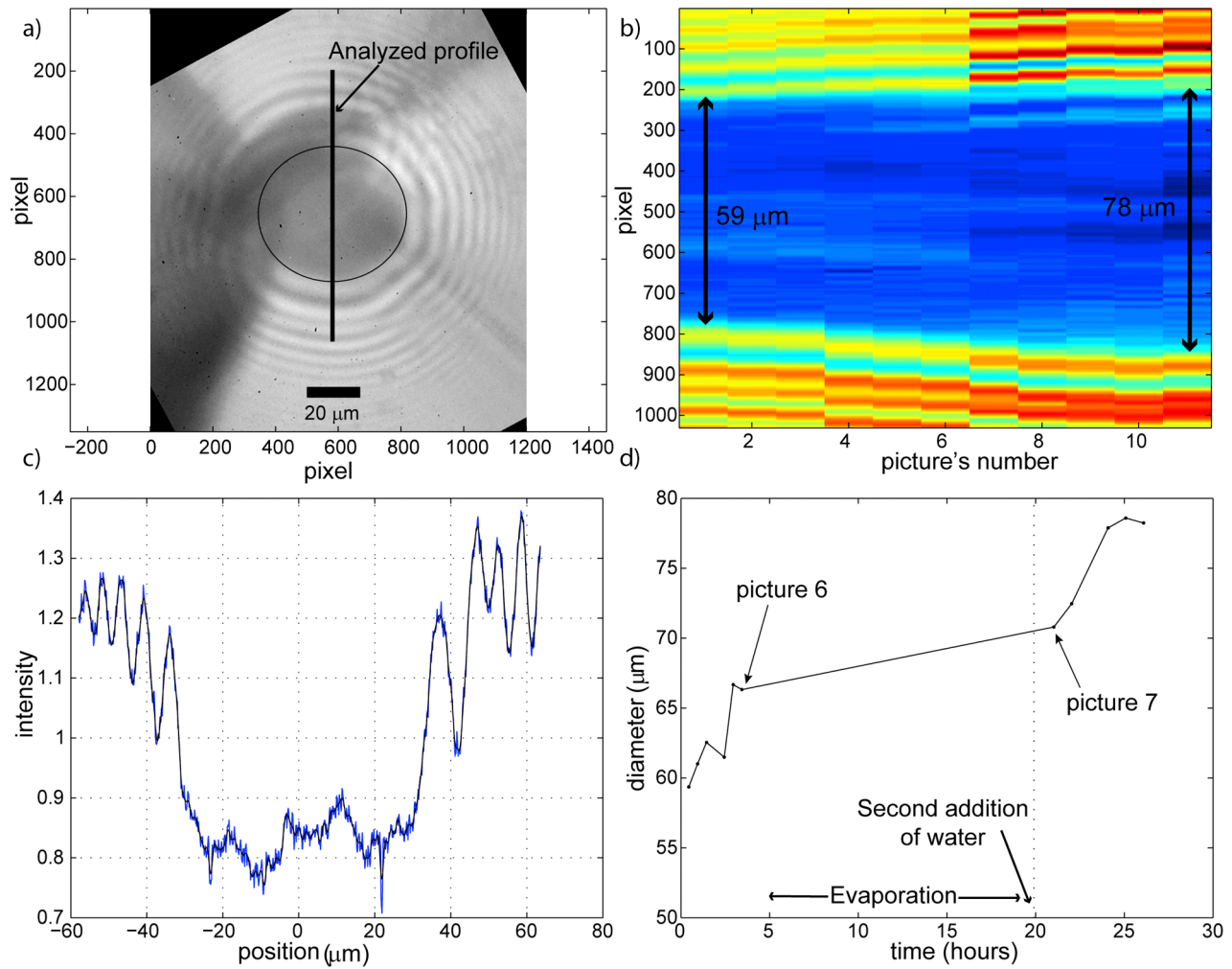


**Figure 3.** Data processing steps of the optical pictures to extract the contact diameter growth rate for experiment F01. (a) Green channel of the first analyzed picture showing the contact surrounded by Newton rings, (b) selected profile for pictures 1 to 11, (c) each profile is filtered and centered on  $X = 0$ , and (d) growth of the diameter through time.

[19] The volume of dissolved calcite is then converted into a number of moles,  $N = V_i * \rho / M$ , where  $\rho = 2.7 \text{ g/cm}^3$  (the density of calcite) and  $M = 100 \text{ g/mol}$  (the molecular mass of calcite). The amount of dissolved calcite was monitored as a function of time using the displacement of the Newton rings. For each experiment,  $\delta_{i,n}$ ,  $Z_{i,n}$  and  $V_{i,n}$  were calculated for the first two Newton rings,  $n = 1$  and  $n = 2$ . The rate of calcite dissolution in mol/s could then be calculated as a function of time and applied stress. Strain rates,  $\dot{\epsilon}$  in  $\text{s}^{-1}$ , were calculated from the increase of in situ vertical displacement values through time,

$$\dot{\epsilon} = \frac{\Delta Z / R_{eq}}{\Delta t} \quad (4)$$

$R_{eq} = \sqrt{((S_i + S_f) / 2) / \pi}$  being the equivalent contact radius, i.e., diffusion path, taken as a reference length,  $S_i$  and  $S_f$  are the initial and final surface areas of contact, respectively. Two phases could be differentiated in the results for experiments F01, F02, F05, F06 and F07, two strain rates are therefore calculated for these experiments.

### 3.2. White Light Interferometry Measurements

[20] Microstructures that developed during experiments below the indenter were analyzed at the end of each experiment, using digital elevation images obtained from white light interferometry. To improve the quality of the results and their interpretation, linear tilts inherent to the system and samples were removed, and pixels with no signal were interpolated. Surface areas of contact at the end of experiments,  $S_{wli}$ , were then outlined by hand on the digital elevation image using image processing software (Figure 4 and Table 1). Surface areas measured this way include only the part of the contact where enough dissolution occurred to be clearly identified, therefore stress values calculated using these surface areas would represent maximum stress. The actual applied stress therefore lies between the value calculated from the in situ measurements and the one calculated from the white light interferometry measurements.

[21] Instantaneous plastic deformation occurred when the force was applied on calcite crystals. To determine the

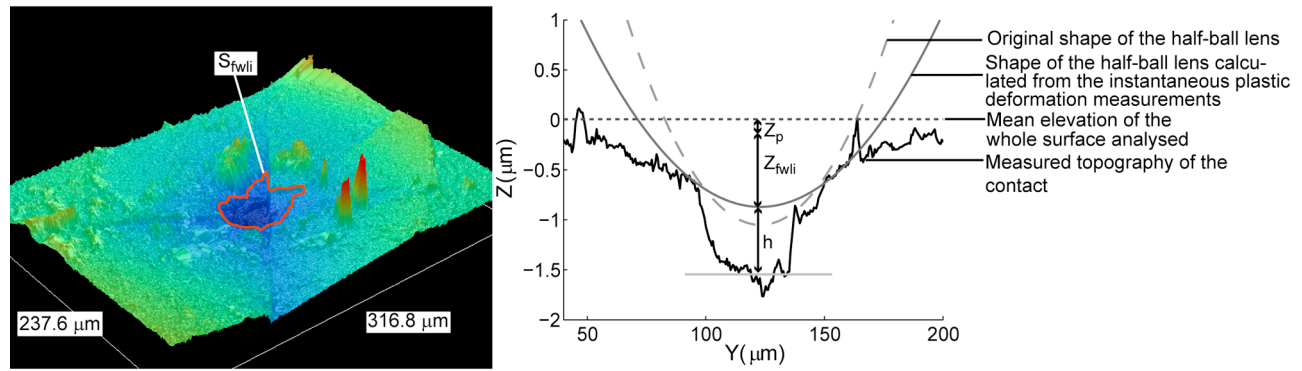


**Figure 4.** Digital elevation image where the contact surface area  $S_{fwli}$  is outlined in red. Values of  $Z_{fwli}$  and  $h$  are calculated from profiles extracted from digital elevation images.

magnitude of dissolution due to pressure solution as revealed by the white light interferometry profiles, the residual imprint of the indenter after instantaneous plastic deformation was measured, and removed. Dry tests were performed in which a calcite sample was loaded and unloaded in the same conditions as in the experiments, i.e., similar crystals, applied forces and half-ball lenses. These tests enabled determination of the residual deformation in the crystal. The residual holes were fitted with circles of radius  $R_{res}$  (see Table 1). The equivalent shapes of the indenter represented on the vertical profiles obtained from white light interferometry measurements have radius  $R_{res}$ . For each half-ball lens, the depth of the residual hole resulting from plastic deformation,  $Z_p$ , was measured. The volume of the residual hole,  $V_p$ , was calculated from  $Z_p$  and  $R_{res}$ . The vertical displacement due to pressure solution creep,  $Z_{fwli}$ , was calculated as being the penetration of the equivalent sphere into

the resulting hole minus the penetration depth,  $Z_p$ , due to plastic deformation (Figure 4).

[22] For most of the experiments the hole created by dissolution of the calcite is deeper than the penetration of the half-ball lens; in these cases the height,  $h$ , of the hole below the indenter was measured (Figure 4). The total volume of the hole,  $V_{fwli}$ , from which  $V_p$  was subtracted, includes both the volume of calcite replaced by the half-ball lens and the volume of calcite dissolved below. Therefore the value of  $V_f$  which includes only the volume of calcite replaced by the half-ball lens (equation (3)) can not be compared to  $V_{fwli}$ . To get an idea of the three-dimensionality of the contact, two topography profiles, perpendicular to each other, were taken for each experiment. For these two profiles of the same surface, the half-ball lens was fitted so that  $Z_{fwli}$  is identical. In the case of noisy profiles an average profile was calculated including the data from the entire hole. The calculated shape

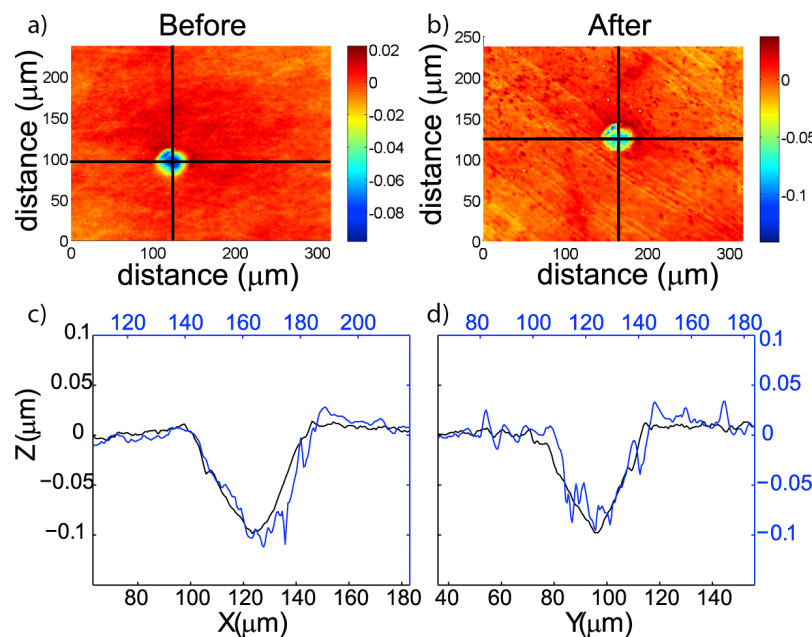


**Figure 5.** (a) Calcite surface after dry deformation with a sapphire half-ball lens of radius 0.500 mm and an applied force  $F = 0.82$  N. (b) Same surface after 50 hours in water saturated with respect to calcite. (c and d) Corresponding topography profiles. The black lines correspond to the measurements before the water treatment and the blue lines correspond to the measurements after the water treatment.

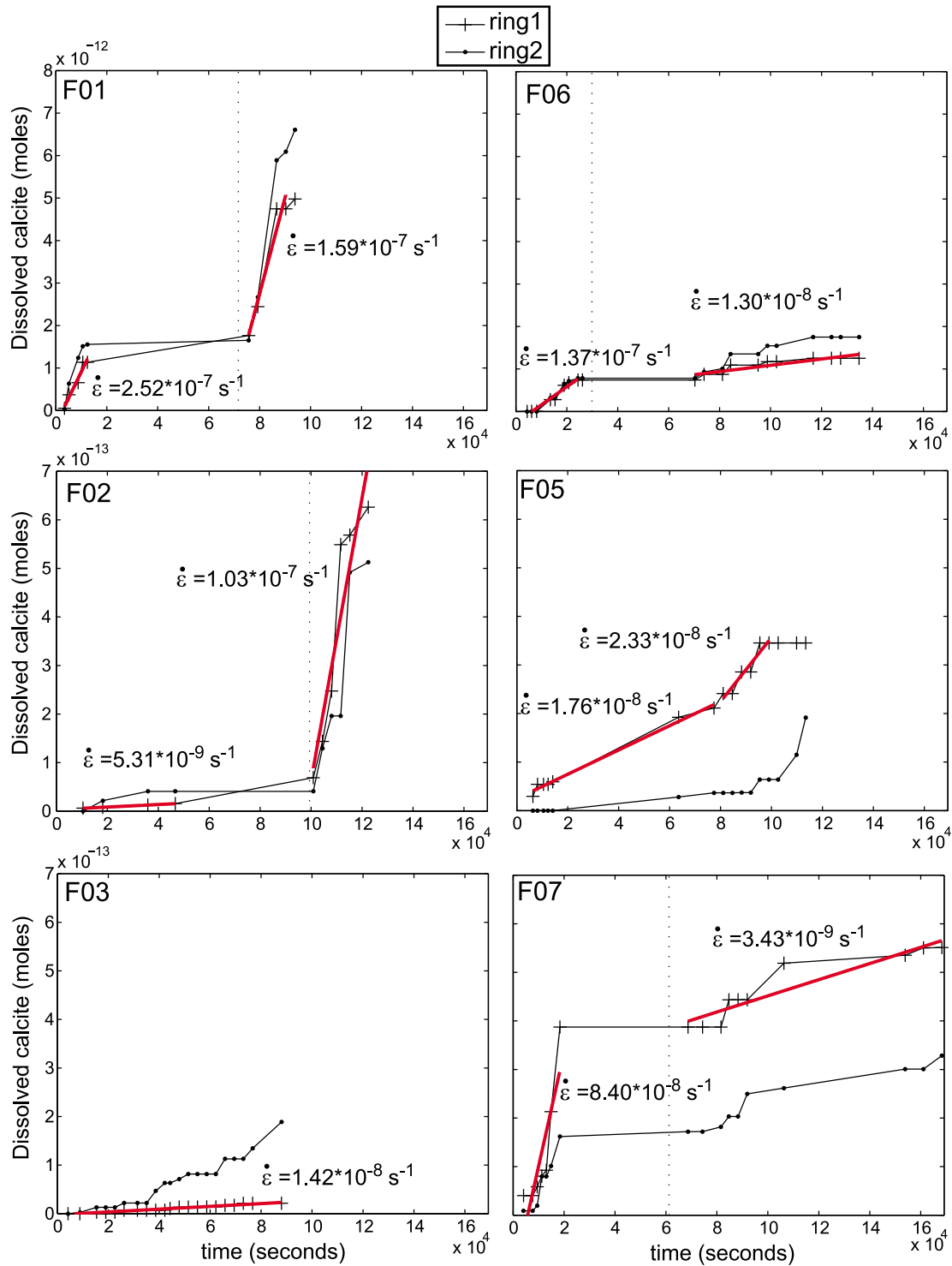


**Figure 6.** Volume of calcite dissolved as a function of time. Vertical dashed lines represent the time at which water was added after the initial water had evaporated in experiments F01, F02, F06 and F07. Strain rates were calculated using data from the first Newton ring (ring 1). Strain rates values are displayed next to each curve, and the red lines correspond to the data interval taken into account when calculating strain rates.

of the half-ball lens was fitted onto this average profile. Therefore some points of the white light interferometry profiles can be located above the line symbolizing the half-ball lens.

[23] The holes observed after the experiments are deeper than the penetration depth of the indenter. Two explanations are possible: this is either due to the stress application or to the dissipation of stored plastic strain energy, i.e., disloca-

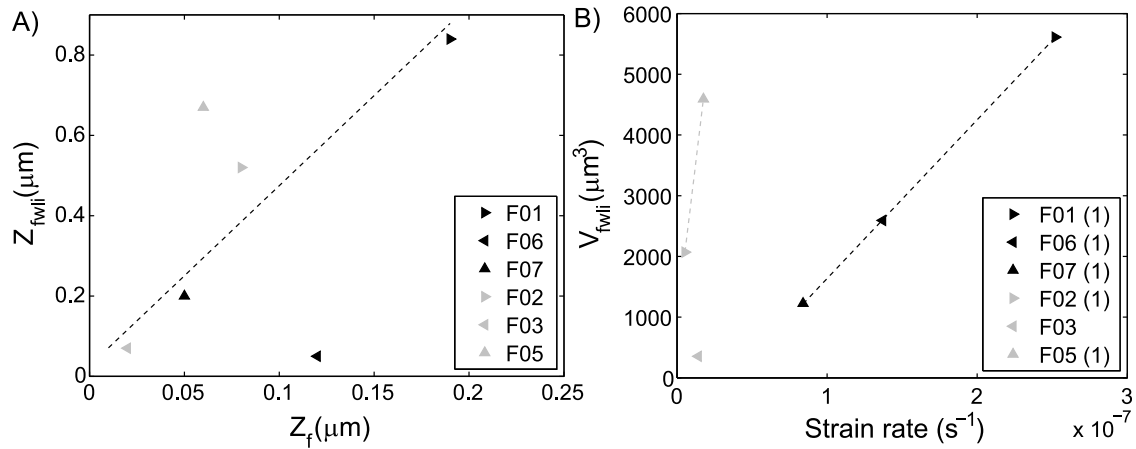


**Figure 7.** Comparison of in situ and ex situ measurements. (a) Ex situ penetration of the half-ball lens as a function of the in situ measurements. (b) Ex situ volume of calcite dissolved as a function of the strain rates for the first part of the experiments.

tions inducing dissolution. To determine which of these two explanations applies, wet tests were performed. Once the residual deformation due to dry indentation was measured, some crystals were left in water saturated with respect to calcite for 50 hours, without any load. At the end of the tests, some crystal reorganization was observed but the depth and shape of the holes was the same as before the water treatment (Figure 5). This implies that the dissolution of calcite below the indenter and under stress is related to the applied stress, i.e., dissolution and precipitation under the effect of a stress-driven mechanism.

## 4. Results

### 4.1. In Situ Vertical Displacements

[24] For each experiment,  $Z_i$  and  $V_i$  were calculated using the displacements of the two first Newton rings (Figure 2). Discrepancy may exist if the vertical displacements are calculated using either the first or the second Newton ring. Trends are, however, rather similar for the two rings and, except for experiments F05 and F07, the results obtained are within the same order of magnitude (Figure 6). Overall, noise is more important in data obtained using the second Newton ring, therefore, all the values of vertical displacement and volume of calcite dissolved, found in Table 1, were calculated using the displacement of the first Newton ring. For experiments F01, F02, F06 and F07 the water film at the contact evaporated during experiments; dissolution started again when water was added once more to the system (Figure 6). In addition, no deformation was observed before water was added to the system, thus it can be concluded that the observed deformations in the present study are due to dissolution of calcite under the effect of stress.

[25] Since lenses with different diameters were used (Table 1), comparison between the different experiments is easier when vertical displacements are converted into number of moles of calcite dissolved. Evolution of calcite dissolution is then followed through time (Figure 6). Strain rates for the different phases of experiments are displayed next to the dissolution versus time curve (Figure 6). In all experiments surface areas of contact increase with time (see

$S_1$  and  $S_f$  in Table 1), therefore applied stresses decrease accordingly. In experiment F01, dissolution is rather constant throughout the experiment. In this case the strain rate is insensitive to the stress variation. In experiments F06 and F07, the second parts of experiments are characterized by slower strain rates. For these two experiments strain rate slows down with decreasing stress. Hence, the decrease in stress is more important in F07 and the decrease in strain rate is also more important in F07 than in F06 (Figure 6). Conversely, the strain rate in F02 increases with decreasing stress. In experiment F05, the strain rate increases after the seventieth hour while stress is decreasing, and after the 27th hour no more deformation is observed (Figure 6). In experiment F03, very little but constant deformation is observed.

[26] Precipitated calcite was observed on crystal surfaces after all experiments. It is, however, difficult to differentiate precipitation due to evaporation of the fluid from precipitation resulting from pressure solution. Quantification of the amount of calcite which precipitated due to pressure solution was therefore not possible.

### 4.2. Roughness of the Interface and Damage

[27] Vertical displacements of the lens into the crystal as measured by white light interferometry are always greater than those obtained from in situ measurements, i.e.,  $Z_{fwli} > Z_f$  (Table 1 and Figure 7). The load was not removed between the two measurements, therefore the discrepancy between the two results is possibly related to the time gap between the end of in situ measuring and taking the white light interferometry measurements and also to the fact that dissolution started right after water was added to the system before the first picture was taken. That is to say  $Z_{fwli} > Z_f$  may be attributed to the fact that dissolution under stress starts before the first in situ measurements and continues in between the two measurements. Overall  $Z_{fwli}$  and  $Z_f$  follow a similar trend, values for experiments F06 and F05 are, however, rather dissimilar (Figure 7). To some extent the discrepancy can be attributed to the different accuracy of the two measurement methods.

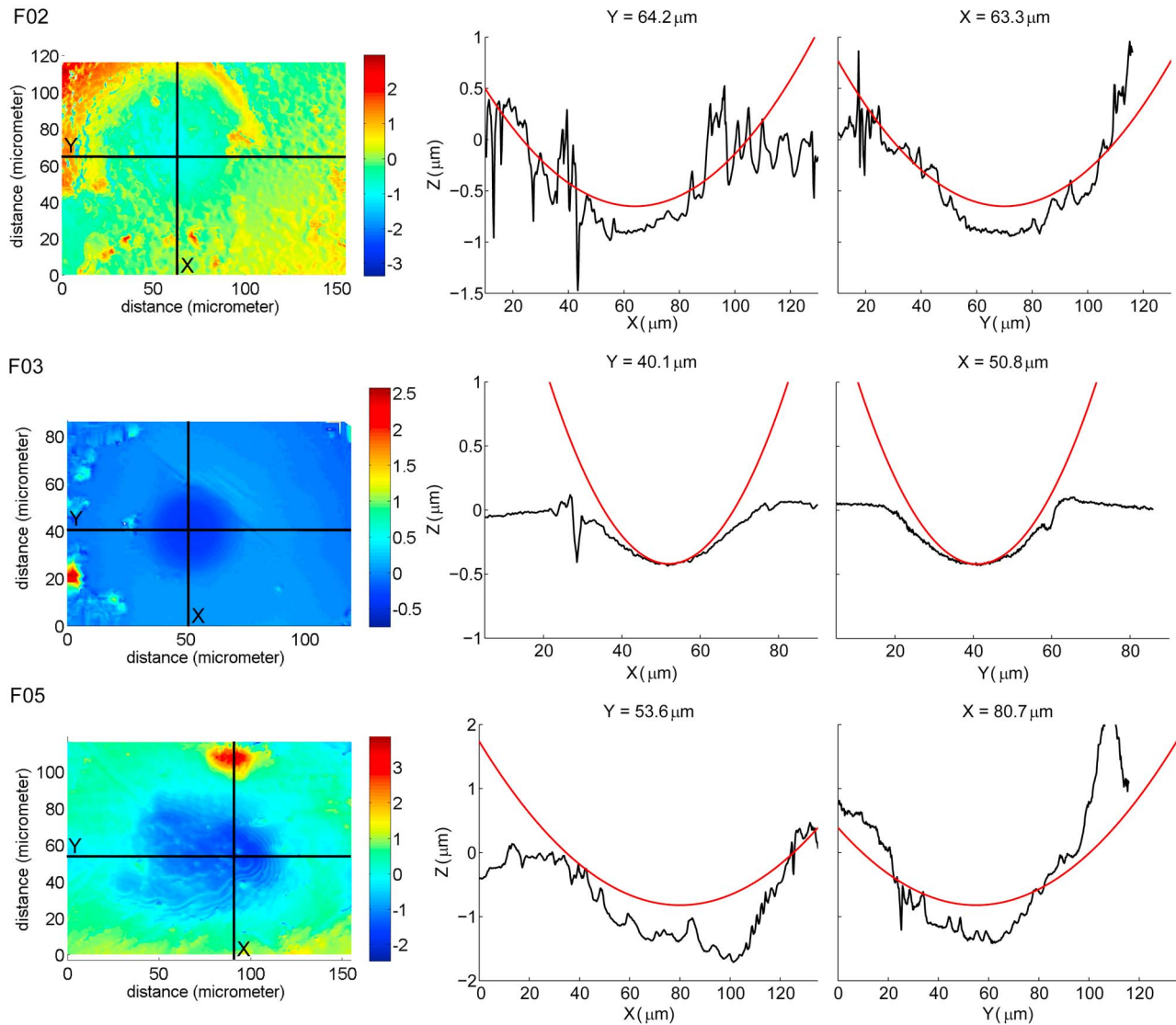


**Figure 8.** Observation by white light interferometry of the contact after experiments F02, F03 and F05. For each experiment the surface topography (color scale bar in micrometers) and two vertical profiles are shown. The red line on the vertical profiles corresponds to the shape of the equivalent half-ball lens. Note the difference of scale between the horizontal and vertical axes.

[28] Two families of contact structure were differentiated from the vertical profiles of the contact and the half-ball lens fitted on it, depending on the presence or absence of cracks crossing the contact. Comparing the volume of dissolved calcite measured ex situ,  $V_{fwtis}$ , with in situ strain rates two trends appear corresponding to the two families of contact (Figure 7). Experiments F02, F05 and, to some extent, F03, are examples of the first type of contact obtained during pressure solution in the present study, where roughness develops within the contact and the shape of the holes observed in vertical profiles closely resemble the shape of the half-ball lens indenter (Figure 8). Observation by scanning electron microscopy of crystal surfaces after experiments did not reveal any cracks. Therefore, in those experiments, dissolution and associated diffusion of matter outside the stressed surface area of contact most likely occurred along the calcite/indenter interface.

[29] Experiments F01, F06 and F07 are examples of the second type of contact obtained during pressure solution in the present study. In these experiments a hole developed below the indenter (Figure 9). Associated with this feature, radial cracks emanating from the contact were observed using scanning electron microscopy (Figure 10). The depth,  $h$ , of the hole below the indenter tends to increase with time (Table 1), leading to the conclusion that the growth of cracks below the indenter is also time dependent. In addition, crack propagation was observed during in situ measurements of experiment F01.

[30] The two types of contact geometry possess one common feature: the indenter does not reach the bottom of the hole created by pressure solution during indentation of the crystal. Pressure solution experiments were also conducted on halite. Halite was indented by glass in the presence of water saturated with respect to halite; the diameter of

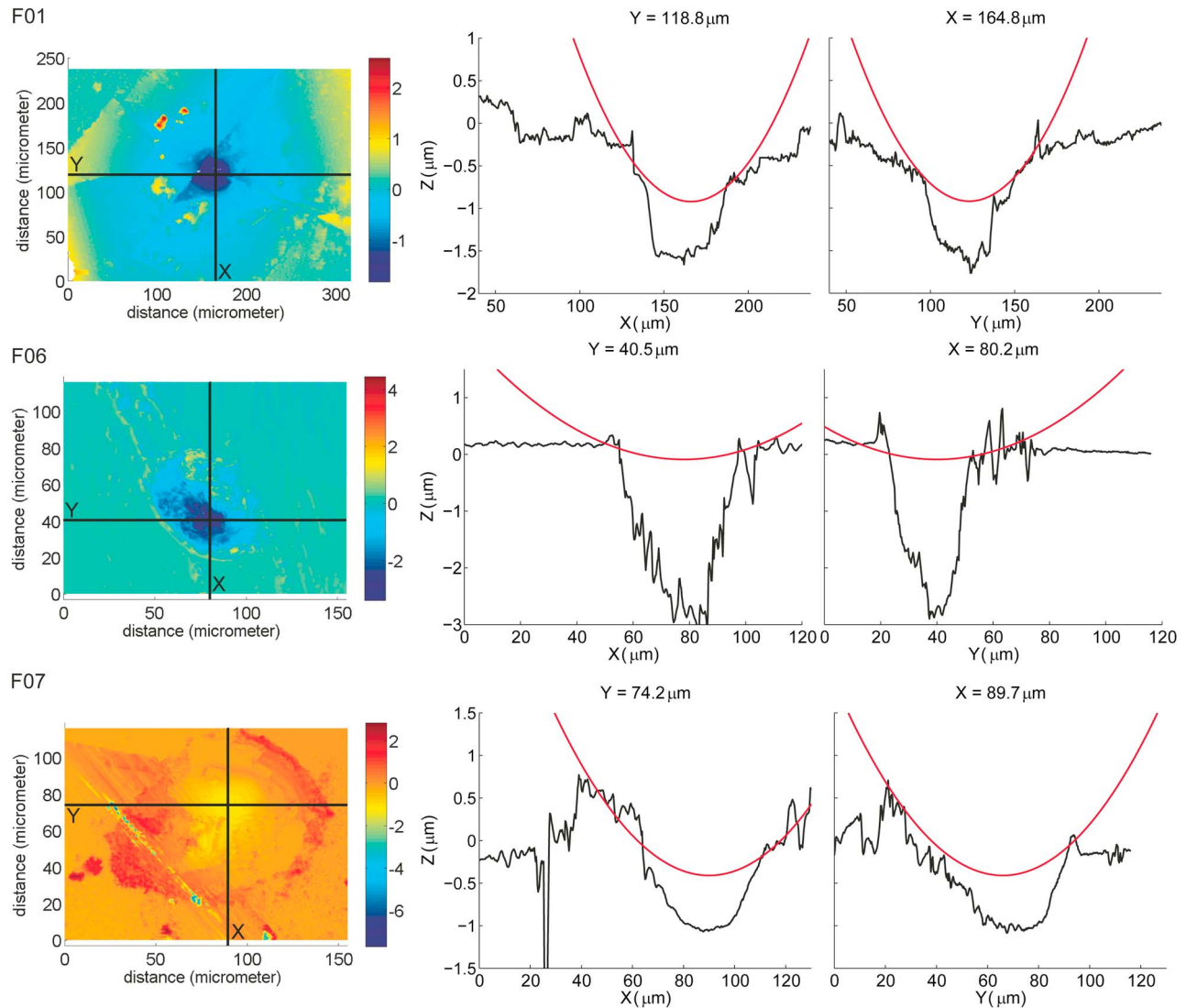


**Figure 9.** Observation by white light interferometry of the contact area after experiments F01, F06 and F07. For each experiment the surface topography (color scale bar in micrometers) and two vertical profiles are shown. The red line on the vertical profiles corresponds to the shape of the equivalent half-ball lens. Note the difference of scale between the horizontal and vertical axes.

the spherical indenter was about  $100 \mu\text{m}$  (Figure 11). Experiments were conducted at various temperatures, and with load applied over several days. In all the experiments on halite a hole was present under the indenter, as observed in Figure 11.

[31] Using information from both in situ and white light interferometry measurements, it is observed that experiments in which a crack propagate under the indenter are characterized by higher rates of dissolution (Figure 12).

## 5. Discussion

[32] Topographic profiles taken using white light interferometry show that two different mechanisms have controlled dissolution and diffusion in the present experiments. During the first phase of the in situ measurements strain rates can also be split in the two same groups. Deformation occurs either by dissolution and transport along the contact

interface, i.e., pressure solution, or by a combination of pressure solution and subcritical crack growth.

### 5.1. Deformation by Pressure Solution

[33] Experiment F03 is characterized by very little deformation and a very flat lens/calcite interface. Moreover, the shape of the hole is almost exactly the shape of the indenter, as should be the case for purely plastic deformation. It is therefore questionable whether or not pressure solution was active in this experiment. However, for experiments F02 and F05, the combination of the rate of indentation and the observation of the topography profiles of the contact at the end of experiments strongly indicates that deformation by a pressure solution mechanism was active. Indentation of calcite occurred by dissolution and diffusion along the lens/calcite interface (Figure 8).

[34] Even though this is at the limit of the data resolution, it is observed that the lens did not reach the bottom of the

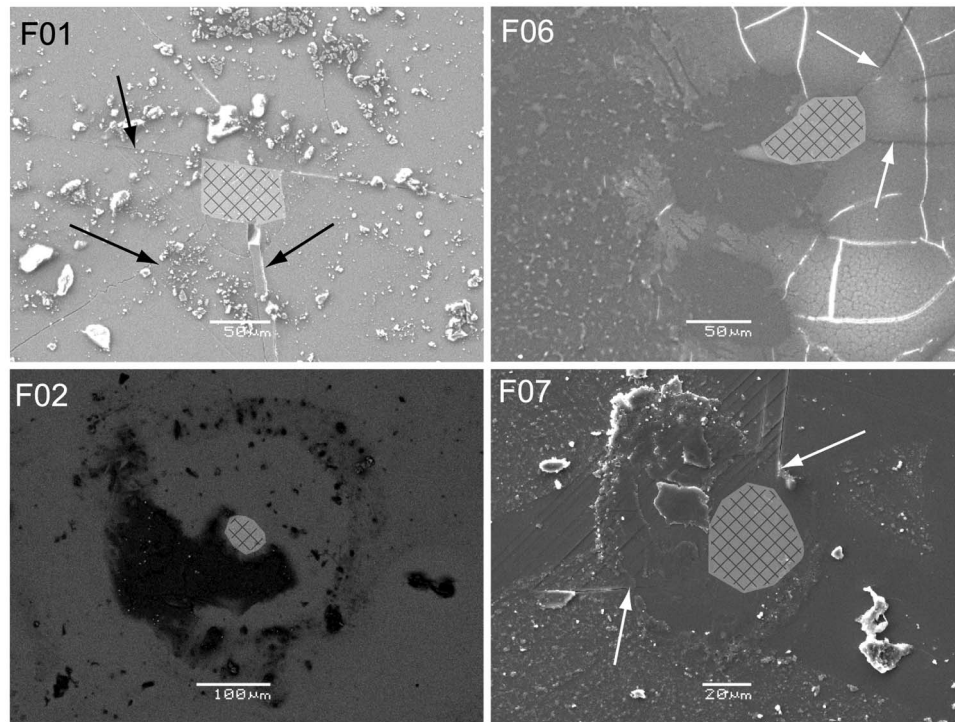


**Figure 10.** Scanning electron micrographs of the crystal surfaces after experiments F01, F02, F06 and F07. Hatched areas represent approximate surface areas of contact during experiments; since the vertical resolution of the scanning electron microscope is low, the areas were determined by comparing these pictures with the white light interferometry data. The arrows point to cracks which start at the contact and continue beyond the contact area. The white flecks on pictures of F01 and F07 contacts correspond to calcite precipitation.

hole created by dissolution of calcite during experiments (Figure 8). Two different hypotheses concerning the way the interface develops, may be drawn from this observation. First, the space between the indenter and the crystal may be attributed to the roughness of the interface. Roughness develops at the stressed crystal/fluid interface due to the thermodynamic instability of a flat solid/fluid interface [Srolovitz, 1989; Angheluta *et al.*, 2009]. In this case the roughness amplitude would be equivalent to the measured value  $h$ , 0.20 and 0.45  $\mu\text{m}$  for F02 and F05, respectively.

Coarsening of a grain boundary structure is related to the stress concentration in the grooves [Koehn *et al.*, 2004]; the same trend is observed in the present experimental study where F05 is characterized by a higher applied stress and a rougher interface. An islands-and-channels structure [Lehner, 1990; Dysthe *et al.*, 2002; den Brok *et al.*, 2002] would then be the most appropriate model to explain the present results. However, the amplitude of the observed roughness is quite large, which might be an indication that the islands-and-channels structure roughened toward a grain

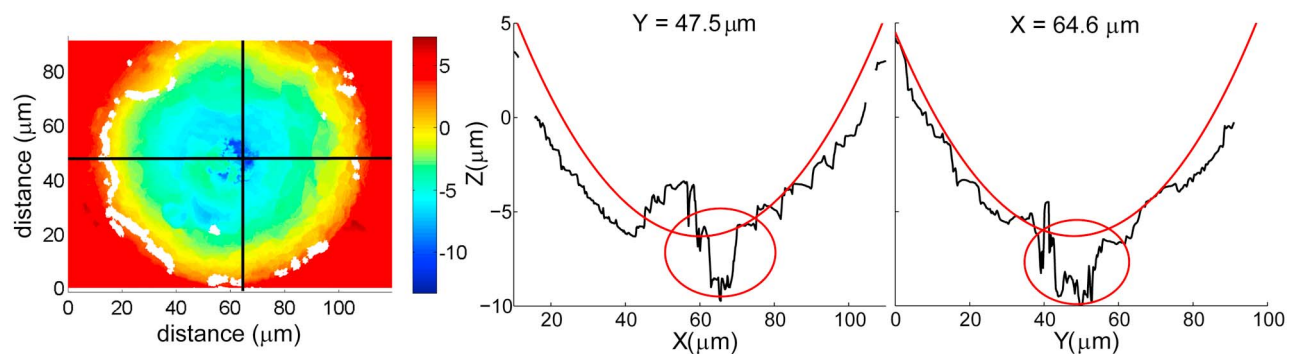


**Figure 11.** White light interferometry surface and topography profiles of a halite crystal indented by glass, approximate shape of the indenter displayed on the profiles. Red circles on both profiles indicate a hole that formed under the indenter. Note the difference of scale between the horizontal and vertical axes.

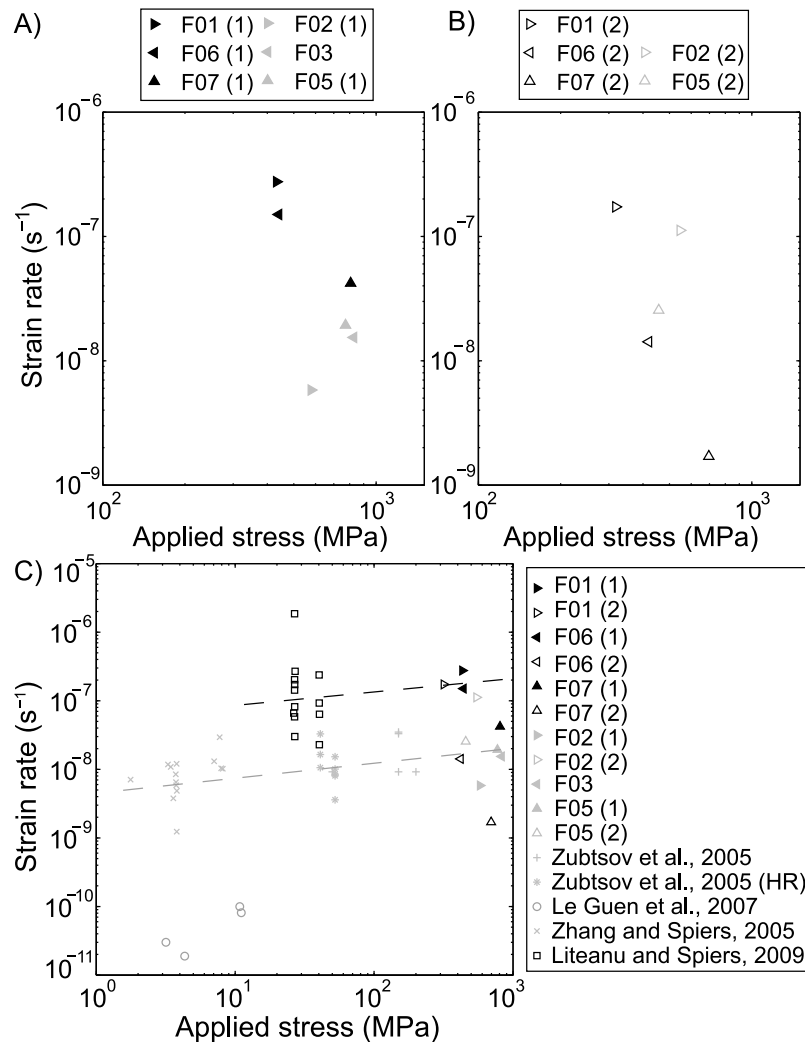


**Figure 12.** Strain rates as a function of the applied stress represented in log-log coordinates. The 1 and 2 in parentheses refer to the stages in strain rate measurements. (a) First phase and (b) second phase of the experiments, as indicated in Figure 6. (c) The present data are compared with data found in other published experiments on carbonates. Experiments in which subcritical crack growth was active are displayed in black. The lines present on the graphs are not regression lines but are present to highlight the increase in strain rate when pressure solution is combined with crack propagation. HR in the legend refers to the high-resolution experiments of *Zubtsov et al.* [2005].

boundary structure as described by *Koehn et al.* [2006], for which the amplitude of the roughness might be of the order of one micrometer. The mean profile roughness under the indenter is of  $0.11 \mu\text{m}$  for F02 and of  $0.18 \mu\text{m}$  for F05. The slightly greater roughness correlates with higher strain rate for the first phase in experiments F02 and F05 (Figure 6), which is in agreement with similar results on quartz [*Gratier et al.*, 2009].

[35] Secondly, the space between the indenter and the crystal may be attributed to the development of a hole in the crystal below the indenter. In this case dissolution of calcite under the indenter must be attributed to the high strain energy stored in the crystal. Previous experimental studies have shown dissolution of free surfaces driven by strain energy [*den Brok and Morel*, 2001; *Koehn et al.*, 2004; *Bisschop and Dysthe*, 2006]. The control experiments with indentations in water, but with no load, shows that it is not

the energy stored by defects, but strain energy due to the load applied by the indenter that drives the dissolution. The observed hole would then be a way for the crystal to lower the energy of the system. Similar observations were made on halite crystals that were indented by glass half-ball lenses (Figure 11) using a similar experimental setup as for the calcite crystals.

## 5.2. Deformation by a Combination of Pressure Solution and Subcritical Crack Growth

[36] In experiments F01, F06 and F07, the depth of the hole below the indenter is of the same order or greater than the penetration depth of the indenter into the crystal (Figure 9 and Table 1). This implies that the same amount, or more, of calcite was dissolved under the indenter than calcite that was replaced by the indenter. Since cracks are observed on both optical and scanning electron microscope images (Figure 10),

in these cases the hole present under the indenter might be due to a combination of dissolution and crack propagation. In brittle material subjected to high stresses, a zone of inelastic deformation immediately below the contact area may develop, leading to the formation of what are called 'vent cracks' [Lawn and Wilshaw, 1975]. Dissolution of minerals occurs preferentially at active sites such as edges, dislocations or microfractures [Lasaga, 1981; Schott et al., 1989]. In the present experiments, the hole below the lens may therefore be a result of the combination of crack development due to high stresses associated with dislocation plasticity, and dissolution of material in the presence of a reactive fluid. While cracks crossing contacts in experiments F06 and F07 remained stable throughout experiments, in F01 crack propagation occurred during the experiment. This observation might explain why strain rate is rather constant in experiment F01 while it diminishes in experiment F06 and F07.

[37] The presence or absence of cracks below the indenter cannot be explained from the present experimental conditions. The two most important parameters controlling crack propagation are the applied tensile stress and the size of the flaw [Anderson, 1995]. Experiments in which a crack propagates below the indenter are not characterized by higher applied stresses than in the other experiments. Therefore, the propagation or not of a crack, in the present study, is probably due to the presence or absence of a flaw in the crystal below the indenter. This hints to the possibility that density of flaws is as important for strain rate as stress itself. However, it must be taken into consideration that the loads and the contact stresses have been varied by less than a factor 2. A systematic study of the development of contact fractures for a wide range of stresses and flaw densities might be useful.

### 5.3. Rate-Controlling Step

[38] Although too little data are available to draw any firm conclusion about the relationship between dissolution and applied stress, it does appear that subcritical crack growth and pressure solution are characterized by different strain rates. Strain rates in experiments in which crack propagation occurred are two orders of magnitude higher than for experiments in which diffusion occurs only through the rough lens/calcite interface (Figures 7 and 12).

[39] Experiments in which evaporation occurred are characterized by two strain rates (Figure 6). For F01, F06 and F07 the rate of dissolution was either constant or decreased after evaporation. The fast initial rate of deformation might indicate that at first crack propagation controls the vertical displacement of the indenter, while continued vertical displacement of the lens becomes increasingly controlled by the rate of dissolution of calcite at the contact points between the lens and the crystal.

[40] Conversely, the rate of dissolution in experiments F02 and F05 increases during the second phase. In these experiments, no cracks crossed the contact, therefore diffusion must occur through the thin film present at the interface. The thickness of the water film might be related to the deviatoric stress at the grain-to-grain contact [Renard and Ortoleva, 1997], while in the case of the islands-and-channel structure the decrease of stress might lead to an increase of the water film thickness, which enables faster

diffusion and therefore a greater strain rate. In experiments in which crack propagation occurred, diffusion proceeded through the crack and was not limited by the applied stress.

[41] If the rate of pressure solution is controlled by diffusion, the displacement rate of the half-ball lens,  $dZ/dt$ , as a function of the measured diameter,  $d$ , may be expressed as,  $dZ/dt = \alpha/d_i^2$  in cases where the applied stress is constant [Weyl, 1959]. In the present study the applied force is constant, but not the stress. Therefore the displacement rate of the half-ball lens as a function of the diameter,  $d$ , may here be expressed as

$$\frac{dZ}{dt} \approx \alpha \frac{1}{d_i^4}, \quad (5)$$

in which  $\alpha$ , in  $\mu\text{m}^3/\text{s}$ , is mainly a function of the lens/calcite interface geometry and thickness,  $\Delta$ , and of the diffusion coefficient,  $D$ , i.e.,  $\alpha \sim D\Delta$ . For all experiments, the relationship between diffusion path diameter and rate of deformation was tested. However, it was difficult to firmly conclude on whether the diameter influence on the vertical displacement rate was of the form  $1/d^2$  or  $1/d^4$ . Therefore it is not possible to conclude whether or not diffusion was the rate-limiting step for pressure solution in the present experiments.

### 5.4. Comparison With Other Studies

[42] Strain rates obtained in this study are in agreement with those obtained in other studies, and three different trends can be observed (Figure 12).

[43] Numerous strain rate laws describing deformation of minerals or aggregates by pressure solution have been derived [Weyl, 1959; Rutter, 1976; Lehner, 1990; Spiers et al., 1990], even though they contain various dissimilarities they all describe the strain rate as positively correlated to the applied stress. However, strain rate data in Figure 12 do not display a strong dependency on applied stress. Experiments in which pressure solution is assumed to be the main process controlling deformation are characterized by a slight increase in the strain rate as stress is increasing [Zhang and Spiers, 2005a; Zubtsov et al., 2005]. However, at the same applied stress the effect of grain size or pore fluid might have a much stronger effect than the variations in applied stress on the strain rate.

[44] Fracture development during slow sediment compaction increases the pressure solution strain rate [Gratier et al., 1999]. Published experiments on calcite in which crack propagation occurred [Liteanu and Spiers, 2009] are characterized by slightly higher strain rates than experiments for which pressure solution was the main mechanism of compaction. This feature was also observed within the present experimental results (Figure 12). From the wide range of experimentally measured strain rates, it can be deduced that the variation of strain rates is mostly a function of the processes active during chemical compaction, i.e., pressure solution or subcritical crack growth, rather than of the applied stress.

[45] As mentioned by Tada and Siever [1989, and references therein], early cementation has an inhibiting effect on intergranular pressure solution. This feature is clearly observed in Figure 12 where cemented rocks deforming by pressure solution [Le Guen et al., 2007] exhibit strain rates

that are 2 to 3 orders of magnitude lower than for aggregates. Faster strain rates observed in aggregates or in the present study might in nature be associated with compaction of loose carbonate sediments or compaction of fault gouges.

## 6. Conclusion

[46] This is the first study that compares results of calcite slow deformation, from nanometer resolution techniques both in situ and ex situ. From these results it was possible to identify the relative importance of pressure solution driven by normal load, and free surface dissolution driven by strain energy, and how these mechanisms couple to mass transport in fluid films and fractures.

[47] The present experimental study enabled the determination of two different processes occurring during pressure solution of calcite crystals at the grain scale. In half of the experiments, diffusion of the dissolved solid took place in the pore fluid present along a rough interface between calcite and the indenter. In the other half of the experiments, diffusion occurred through cracks that propagated from the contact toward the less stressed part of the crystal. The occurrence of one or the other mechanism does not appear to be ruled by the applied stress but is most likely dependent on the presence or not of a flaw in the crystal.

[48] Strain rates are higher for experiments in which crack propagation occurred. The present calculated strain rates are in agreement with the ones obtained in other studies. Overall it seems strain rates are not really stress dependent but rather dependent on the grain size or whether crack propagation occurs or not. The first main difference in strain rates is to be seen between experiments conducted in rock, for which strain rates are three orders of magnitude lower than experiments conducted in aggregates. Within experiments conducted on aggregates or single crystals, when crack propagation occurs strain rates increase by one to two orders of magnitude.

[49] **Acknowledgments.** We would like to thank J. P. Gratier for fruitful discussions. Olav Gundersen is thanked for his help in the laboratory. Reinier van Noort and an anonymous reviewer are thanked for their positive and constructive reviews.

## References

- Anderson, T. L. (1995), *Fracture Mechanics: Fundamentals and Applications*, 2nd ed., CRC Press, Boca Raton, Fla.
- Angevine, C. L., D. L. Turcotte, and M. D. Furnish (1982), Pressure solution lithification as a mechanism for the stick-slip behavior of faults, *Tectonics*, *1*(2), 151–160, doi:10.1029/TC001i002p00151.
- Angheluta, L., E. Jettestuen, and J. Mathiesen (2009), Thermodynamics and roughening of solid-solid interfaces, *Phys. Rev. E*, *79*(3), 031601, doi:10.1103/PhysRevE.79.031601.
- Atkinson, B. K. (1982), Subcritical crack propagation in rocks: theory, experimental results and applications, *J. Struct. Geol.*, *4*(1), 41–56, doi:10.1016/0191-8141(82)90005-0.
- Baker, P. A., M. Kastner, J. D. Byerlee, and D. A. Lockner (1980), Pressure solution and hydrothermal recrystallization of carbonate sediments: An experimental study, *Mar. Geol.*, *38*(1–3), 185–203, doi:10.1016/0025-3227(80)90058-4.
- Bisschop, J., and D. K. Dysthe (2006), Instabilities and coarsening of stressed crystal surfaces in aqueous solution, *Phys. Rev. Lett.*, *96*(14), 146103, doi:10.1103/PhysRevLett.96.146103.
- De Meer, S., and C. J. Spiers (1999), On mechanisms and kinetics of creep by intergranular pressure solution, in *Growth, Dissolution and Patterns Formation in Geosystems*, edited by B. Jamtveit and P. Meakin, pp. 345–366, Kluwer Acad., Dordrecht, Netherlands.
- den Brok, S. W. J., and J. Morel (2001), The effect of elastic strain on the microstructure of free surfaces of stressed minerals in contact with an aqueous solution, *Geophys. Res. Lett.*, *28*(4), 603–606, doi:10.1029/2000GL011461.
- den Brok, B., J. Morel, and M. Zahid (2002), In situ experimental study of roughness development at a stressed solid/fluid interface, in *Deformation Mechanisms, Rheology and Tectonics: Current Status and Future Perspectives*, edited by S. DeMeer et al., *Geol. Soc. Spec. Publ.*, *200*, 73–83.
- Dysthe, D. K., Y. Podladchikov, F. Renard, J. Feder, and B. Jamtveit (2002), Universal scaling in transient creep, *Phys. Rev. Lett.*, *89*(24), 246102, doi:10.1103/PhysRevLett.89.246102.
- Fischer-Cripps, A. C. (1999), The hertzian contact surface, *J. Mater. Sci.*, *34*(1), 129–137, doi:10.1023/A:1004490230078.
- Gratier, J. P. (1987), Pressure solution-deposition creep and associated tectonic differentiation in sedimentary rocks, in *Deformation of Sediments and Sedimentary Rocks*, edited by M. E. Jones and M. F. Preston, *Geol. Soc. Spec. Publ.*, *29*, 25–38.
- Gratier, J. P., F. Renard, and P. Labaume (1999), How pressure solution creep and fracturing processes interact in the upper crust to make it behave in both a brittle and viscous manner, *J. Struct. Geol.*, *21*(8–9), 1189–1197, doi:10.1016/S0191-8141(99)00035-8.
- Gratier, J.-P., R. Guiguet, F. Renard, L. Jenatton, and D. Bernard (2009), A pressure solution creep law for quartz from indentation experiments, *J. Geophys. Res.*, *114*, B03403, doi:10.1029/2008JB005652.
- Gratz, A. J. (1991), Solution-transfer compaction of quartzites—Progress toward a rate law, *Geology*, *19*(9), 901–904, doi:10.1130/0091-7613(1991)019<0901:STCOQP>2.3.CO;2.
- Griffith, A. A. (1921), The phenomena of rupture and flow in solids, *Philos. Trans. R. Soc. London, Ser. A*, *221*, 163–198, doi:10.1098/rsta.1921.0006.
- Hickman, S. H., and B. Evans (1991), Experimental pressure solution in halite—The effect of grain interphase boundary structure, *J. Geol. Soc.*, *148*, 549–560, doi:10.1144/gsjgs.148.3.0549.
- Hickman, S. H., and B. Evans (1995), Kinetics of pressure solution at halite-silica interfaces and intergranular clay films, *J. Geophys. Res.*, *100*(B7), 13,113–13,132, doi:10.1029/95JB00911.
- Johnson, K. L. (1985), *Contact Mechanics*, Cambridge Univ. Press, Cambridge, U. K.
- Karcz, Z., E. Aharonov, D. Ertas, R. Polizzotti, and C. H. Scholz (2006), Stability of a sodium chloride indenter contact undergoing pressure solution, *Geology*, *34*(1), 61–63, doi:10.1130/G21722.1.
- Koehn, D., D. K. Dysthe, and B. Jamtveit (2004), Transient dissolution patterns on stressed crystal surfaces, *Geochim. Cosmochim. Acta*, *68*(16), 3317–3325, doi:10.1016/j.gca.2004.02.004.
- Koehn, D., A. Malthe-Sorensen, and C. W. Passchier (2006), The structure of reactive grain-boundaries under stress containing confined fluids, *Chem. Geol.*, *230*(3–4), 207–219, doi:10.1016/j.chemgeo.2006.02.026.
- Lasaga, A. C. (1981), Rate laws of chemical reactions, *Rev. Mineral.*, *8*, 1–68.
- Lawn, B., and R. Wilshaw (1975), Indentation fracture—Principles and applications, *J. Mater. Sci.*, *10*(6), 1049–1081, doi:10.1007/BF00823224.
- Le Guen, Y., F. Renard, R. Hellmann, E. Brosse, M. Collombet, D. Tisserand, and J.-P. Gratier (2007), Enhanced deformation of limestone and sandstone in the presence of high  $P_{CO_2}$  fluids, *J. Geophys. Res.*, *112*, B05421, doi:10.1029/2006JB004637.
- Lehner, F. K. (1990), Thermodynamics of rock deformation by pressure solution, in *Deformation Processes in Minerals, Ceramics and Rocks*, edited by D. J. Barber and P. G. Meredith, pp. 296–333, Unwin Hyman, London.
- Liteanu, E., and C. J. Spiers (2009), Influence of pore fluid salt content on compaction creep of calcite aggregates in the presence of supercritical  $CO_2$ , *Chem. Geol.*, *265*(1–2), 134–147, doi:10.1016/j.chemgeo.2008.12.010.
- Olagnon, C., J. Chevalier, and V. Pauchard (2006), Global description of crack propagation in ceramics, *J. Eur. Ceram. Soc.*, *26*(15), 3051–3059, doi:10.1016/j.jeurceramsoc.2005.11.004.
- Raj, R. (1982), Creep in polycrystalline aggregates by matter transport through a liquid-phase, *J. Geophys. Res.*, *87*(B6), 4731–4739, doi:10.1029/JB087iB06p04731.
- Ramsay, J. G. (1980), The crack-seal mechanism of rock deformation, *Nature*, *284*(5752), 135–139, doi:10.1038/284135a0.
- Renard, F., and P. J. Ortoleva (1997), Water films at grain-grain contacts: Debye-Hueckel, osmotic model of stress, salinity, and mineralogy dependence, *Geochim. Cosmochim. Acta*, *61*(10), 1963–1970, doi:10.1016/S0016-7037(97)00036-7.
- Renard, F., J. P. Gratier, and B. Jamtveit (2000), Kinetics of crack-sealing, intergranular pressure solution, and compaction around active faults, *J. Struct. Geol.*, *22*, 1395–1407, doi:10.1016/S0191-8141(00)00064-X.

- Rutter, E. H. (1976), The kinetics of rock deformation by pressure solution, *Philos. Trans. R. Soc. London, Ser. A*, 283(1312), 203–219, doi:10.1098/rsta.1976.0079.
- Rutter, E. H. (1983), Pressure solution in nature, theory and experiment, *J. Geol. Soc.*, 140(5), 725–740, doi:10.1144/gsjgs.140.5.0725.
- Scholz, C. H. (2002), *The Mechanics of Earthquakes and Faulting*, 2nd ed., Cambridge Univ. Press, Cambridge, U. K.
- Schott, J., S. L. Brantley, D. A. Crerar, C. Guy, M. Borsik, and C. Willaime (1989), Dissolution kinetics of strained calcite, *Geochim. Cosmochim. Acta*, 53(2), 373–382, doi:10.1016/0016-7037(89)90389-X.
- Sorby, H. C. (1863), The Bakerian lecture: On the direct correlation of mechanical and chemical forces, *Proc. R. Soc. London*, 12, 538–550, doi:10.1098/rspl.1862.0117.
- Spiers, C. J., P. M. T. M. Schutjens, R. H. Brzesowsky, C. J. Peach, J. L. Liezenberg, and H. J. Zwart (1990), Experimental determination of constitutive parameters governing creep of rocksalt by pressure solution, in *Deformation Mechanisms, Rheology and Tectonics*, edited by R. J. Knipe and E. H. Rutter, *Geol. Soc. Spec. Publ.*, 54, 215–227.
- Srolovitz, D. J. (1989), On the stability of surfaces of stressed solids, *Acta Metall.*, 37(2), 621–625, doi:10.1016/0001-6160(89)90246-0.
- Tada, R., and R. Siever (1986), Experimental knife-edge pressure solution of halite, *Geochim. Cosmochim. Acta*, 50(1), 29–36, doi:10.1016/0016-7037(86)90045-1.
- Tada, R., and R. Siever (1989), Pressure solution during diagenesis, *Annu. Rev. Earth Planet. Sci.*, 17, 89–118, doi:10.1146/annurev.earth.17.050189.000513.
- Tolansky, S. (1973), *An Introduction to Interferometry*, 2nd ed., Longman, London.
- van Noort, R., C. Spiers, and C. Peach (2007), Effects of orientation on the diffusive properties of fluid-filled grain boundaries during pressure solution, *Phys. Chem. Miner.*, 34(2), 95–112, doi:10.1007/s00269-006-0131-9.
- van Noort, R., H. J. M. Visser, and C. J. Spiers (2008), Influence of grain boundary structure on dissolution controlled pressure solution and retarding effects of grain boundary healing, *J. Geophys. Res.*, 113, B03201, doi:10.1029/2007JB005223.
- Weyl, P. K. (1959), Pressure solution and the force of crystallization: A phenomenological theory, *J. Geophys. Res.*, 64(11), 2001–2025, doi:10.1029/JZ064i011p02001.
- Yamasaki, N., and T. Weiping (1993), Hydrothermal hot-pressing of calcium carbonate with sea water, *J. Mater. Sci. Lett.*, 12(7), 516–519, doi:10.1007/BF00452814.
- Yasuhara, H., D. Elsworth, and A. Polak (2003), A mechanistic model for compaction of granular aggregates moderated by pressure solution, *J. Geophys. Res.*, 108(B11), 2530, doi:10.1029/2003JB002536.
- Zhang, X., and C. J. Spiers (2005a), Compaction of granular calcite by pressure solution at room temperature and effects of pore fluid chemistry, *Int. J. Rock Mech. Min. Sci.*, 42, 950–960, doi:10.1016/j.ijrmmms.2005.05.017.
- Zhang, X., and C. J. Spiers (2005b), Effects of phosphate ions on intergranular pressure solution in calcite: An experimental study, *Geochim. Cosmochim. Acta*, 69(24), 5681–5691, doi:10.1016/j.gca.2005.08.006.
- Zhang, X., J. Salemans, C. J. Peach, and C. J. Spiers (2002), Compaction experiments on wet calcite powder at room temperature; evidence for operation of intergranular pressure solution, in *Deformation Mechanisms, Rheology and Tectonics: Current Status and Future Perspectives*, edited by S. de Meer et al., *Geol. Soc. Spec. Publ.*, 200, 29–39.
- Zubtsov, S., F. Renard, J. P. Gratier, R. Guiguet, D. K. Dysthe, and V. Traskine (2004), Experimental pressure solution compaction of synthetic halite/calcite aggregates, *Tectonophysics*, 385(1–4), 45–57, doi:10.1016/j.tecto.2004.04.016.
- Zubtsov, S., F. Renard, J. P. Gratier, D. K. Dysthe, and V. Traskine (2005), Single-contact pressure solution creep on calcite monocrystals, in *Deformation Mechanisms, Rheology and Tectonics: From Minerals to the Lithosphere*, edited by D. Gapais et al., *Geol. Soc. Spec. Publ.*, 243, 81–95.

---

K. Bjørlykke and D. Croizé, Department of Geosciences, University of Oslo, PO Box 1047, Blindern, 0316 Oslo, Norway. (delphine.croize@geo.uio.no)

D. K. Dysthe, Physics of Geological Processes, University of Oslo, PO Box 1048, Blindern, 0316 Oslo, Norway.

F. Renard, LGCA-CNRS-Observatoire de Grenoble, Université Joseph Fourier-Grenoble I, BP 53, F-38041 Grenoble, France.